Journal of Organometallic Chemistry 694 (2009) 3232–3241

Contents lists available at ScienceDirect

Journal of Organometallic Chemistry

journal homepage: www.elsevier.com/locate/jorganchem

Chemically bonded assembly and photophysical properties of luminescent hybrid polymeric materials embedded into silicon–oxygen network and carbon unit

Xiaofei Qiao, Bing Yan *

Department of Chemistry, Tongji University, Siping Road 1239, Shanghai 200092, China

ARTICLE INFO

Article history:
Received 24 March 2009
Received in revised form 26 May 2009
Accepted 16 June 2009
Available online 21 June 2009

Keywords:
Chemically bonded hybrid material
Sol–gel
Organic chain and inorganic network
Photoluminescence

ABSTRACT

Through the reaction between the hydroxyl groups of 2-hydroxyl-3-methylbenzoic acid (HMBA), the glycol (G), the diglycol (DG) or the polyethylene glycol (PEG) and the isocyanate groups of 3-(triethoxysilyl)-propyl isocyanate (TEPIC), the hybrid precursors HMBA-Si, G-Si, DG-Si and PEG-Si were obtained. And then the precursors HMBA-Si and G-Si (DG-Si, PEG-Si) have coordinated to the rare earth ions with the carbonyl group of G-Si (DG-Si, PEG-Si) and the carboxyl group of HMBA-Si to form the hybrid materials HMBA-G-RE-Si (HMBA-DG-RE-Si, HMBA-PEG-RE-Si) through hydrolysis and copolycondensation with the tetraethoxysilane (TEOS) via sol–gel process. Subsequently, the NMR, FT-IR and ultraviolet absorption spectra have indicated that the effective precursors have been obtained successfully and the obtained materials possess the characteristic fluorescent properties, thermal stabilities and regular trunk with hole-like microstructures.

1. Introduction

In recent years, a great deal of attention has been paid to the inorganic–organic hybrid materials due to the unique and peculiar properties. Especially, the rare earth ion-containing hybrid material has played an prominent role in a variety of areas such as biology, dyestuff, fluoroimmunoassays [1,2], electroluminescence devices [3,4], and polymer optical fibers [5,6], as the result of the extremely sharp emission bands, different extent of lifetime, potential high internal quantum efficiency, the extensive range of mechanical, chemical, optical and electronic properties of the hybrid material [7,8]. Considering that the f–f electronic transitions of the rare earth metal ions are forbidden and have the low absorption coefficient in ultraviolet–visible region, in the system of the organic–inorganic hybrid material the organic ligand has been introduced to absorb the light and to transfer the energy to the emitting metal centers (rare earth metal ions). This is called antenna effect, to sensitize the metal ions, increase the absorption cross section and protect metal ions from quenching effect aroused by vibrational coupling of water around [9]. Besides, since the pure organic complex has the poor thermal stability and mechanical properties to restrict the practical application, while the inorganic host has better thermal stability and mechanical resistance but worse luminescent properties, the advantages of combination of both are to obtain the luminescent and mechanical properties simultaneously.

According to the interaction between the rare earth ion-containing organic complex and the inorganic host, the hybrid material has been divided into two major classes by Sanchez et al. [10]. The hybrid material where the organic and inorganic components combine with each other by the weak interactions such as hydrogen bonding, van der Waals force or weak static effects, is called class I, while class II is by the powerful chemical covalent bond [11–15]. In the class I, the two components exist as two separate phases, bringing concentration quenching and the leaching effect of the photoactive molecules (rare earth ions). Besides, the concentration of rare earth organic complex in inorganic host could be limited and it is difficult to obtain transparent and uniform appearance and microstructure. Therefore, the major investigations have been absorbed on class II hybrid material in recent years since it has exhibited monophasic appearance even at a high concentration of lanthanide complexes [16–25]. Moreover, the class II material is located in the molecular-based composite region so that it could protect the emitting metal center from agglomeration to make it more possible to modify the network structure and to obtain other properties of novel multifunctional materials where different components combine with each other through the chemical covalent bonds as a single phase [26].

Many kinds of methods to synthesize the hybrid material have been developed and utilized in different areas. It is shown that the sol–gel method has become a suitable approach to prepare the novel luminescent hybrid material due to its advantages in the operational process such as the low reaction temperature, modification on final shape by controlling the process condition and so on [27,28]. Therefore the rare earth ion-containing organic complexes are protected from moisture and high temperatures

* Corresponding author. Tel.: +86 21 65984663; fax: +86 21 65982287.
E-mail address: byan@tongji.edu.cn (B. Yan).

0022-328X/$ - see front matter © 2009 Elsevier B.V. All rights reserved.
doi:10.1016/j.jorganchem.2009.06.019

when incorporated into inorganic transparent matrices by sol–gel method [29]. In addition, the sol–gel method could realize the versatility of the multifunctional material which possesses the thermal stability, the mechanical strength of silica and the optical characteristic emission. Therefore, in order to combine the merits of the pure emission color of rare earth ion-containing organic complex with the plastic properties of the polymer material, polymer-based rare earth hybrid materials have emerged recently through the sol–gel method [30–34]. Hybrid materials containing the high molecular weight polymer, such as poly(oxyethylene), poly(oxypropylene) and so on, have attracted plenty of interest due to their various practical applications as high energy density batteries, sensors, and electrochromic and photoelectrochemical solid-state devices [35–39].

In this paper, we have brought forward a novel synthetic approach to construct a series of Tb^{3+}, Eu^{3+}-containing polymer-containing hybrid materials. We have modified the organic aromatic ligand and the glycol (diglycol and polyethylene glycol) by employing 3-(triethoxysilyl)-propyl isocyanate (TEPIC), subsequently, the rare earth metal ions have coordinated with them through the carboxyl or carbonyl groups. Moreover, the hydrolysis/polycondensation process has occurred with the siloxane derivatives to form the Si–O network by sol–gel method and obtain the Tb^{3+}, Eu^{3+}-containing hybrid polymers with high molecule weight and luminescent properties.

2. Experimental

2.1. Chemicals

2-Hydroxyl-3-methylbenzoic acid (HMBA) and 3-(triethoxysilyl)-propyl isocyanate (TEPIC) are supplied by Lancaster Synthesis Ltd. Glycol (G), diglycol (DG) and polyethylene glycol (PEG) are purchased from Shanghai chemical plant. Other reagents are analytically pure. Europium and terbium nitrate were obtained by dissolving Eu_2O_3 and Tb_4O_7 in concentrated nitric acid, respectively. Tetraethoxysilane (TEOS, Aldrich) was distilled and stored under nitrogen atmosphere.

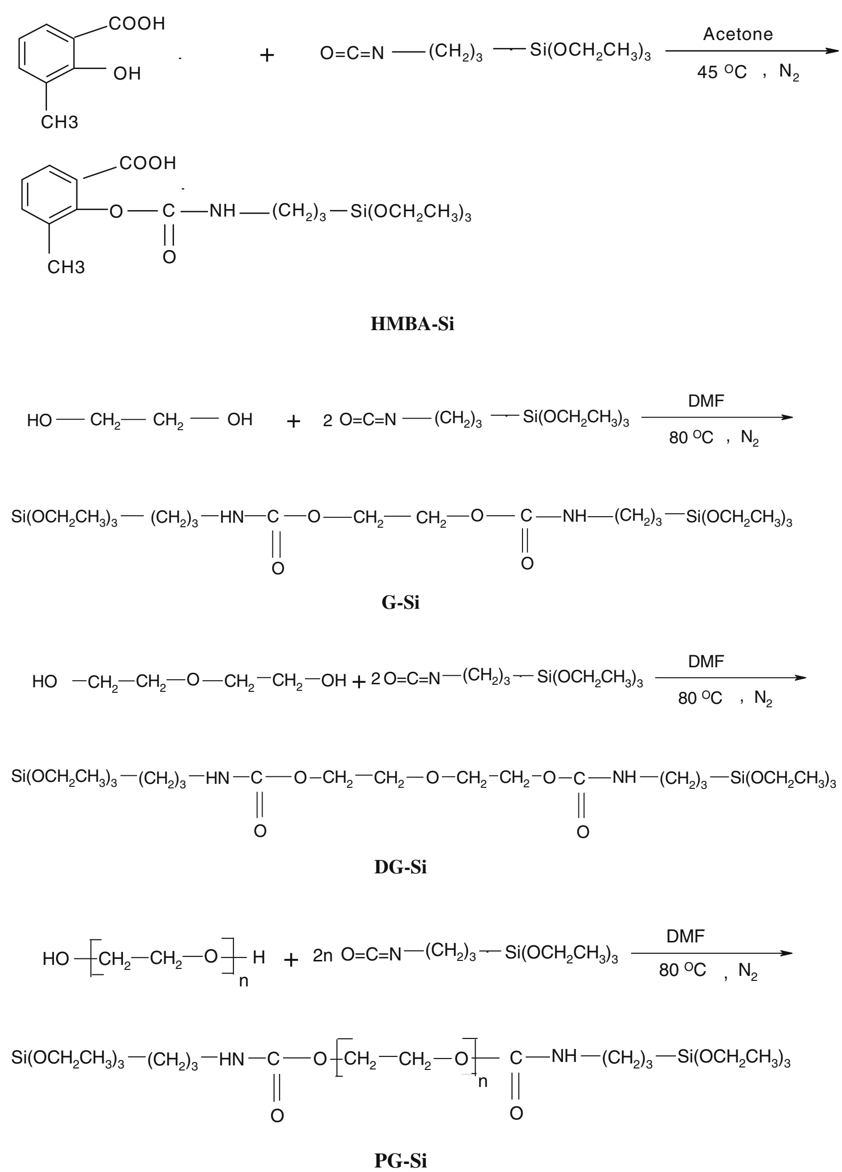

Fig. 1. Scheme of synthesis processes of the precursors (HMBA-Si, G-Si, DG-Si and PG-Si in (a) and hybrid materials (HMBA-G-Si-RE, HMBA-DG-Si-RE and HMBA-PEG-Si-RE in (b).

2.2. Synthesis procedures

Synthesis of the precursor HMBA-Si: 1 mmol (0.152 g) HMBA was first dissolved in acetone solvent completely by stirring, 3-(triethoxysilyl)-propyl isocyanate (1 mmol, 0.243 g) was then added into the solution slowly. After refluxing at 45 °C under nitrogen atmosphere for 12 h the mixture was concentrated to remove the solvent acetone using a rotary vacuum evaporator, and the white powder was obtained. Subsequently, the decontamination processes (precipitation and filtration) were carried on three times by employing the hexane solvent as a purificant. At last the pure white powder (HMBA-Si) was obtained and dried in a vacuum (see Fig. 1a). The ^{1}H NMR data of HMBA-Si ($C_{18}H_{29}NO_7Si$) are as follows: δ0.64 (2H, t), 1.25 (9H, t), 1.68 (2H, m), 2.30 (3H, s), 3.18 (2H, m), 3.84 (6H, m), 4.81 (1H, t), 6.83 (1H, t), 7.38 (1H, d), 7.79 (1H, d), 10.80 (1H, s).

Synthesis of precursor (G-Si, DG-Si and PEG-Si): 2 mmol glycol, diglycol or polyethylene glycol were dissolved in dimethylformamide solvent (DMF) completely by stirring, respectively, 4 mmol (0.990 g) 3-(triethoxysilyl)-propyl isocyanate was then added to the solution slowly. After refluxing at 80 °C under nitrogen for 12 h, the whole mixture was concentrated to remove the solvent acetone using a rotary vacuum evaporator, and the yellow slimy liquid was obtained. Subsequently, the decontamination processes (precipitation and filtration) were carried on three times by employing the hexane solvent as a purificant. At last the pure yellow liquid samples were obtained and dried in a vacuum (G-Si, DG-Si, PEG-Si) (see Fig. 1a). The 1H NMR data of DG-Si ($C_{24}H_{52}N_2O_{11}Si_2$) are as follows: δ0.71 (4H, t), 1.22 (18H, t), 1.81 (4H, m), 3.25 (4H, m), 3.47 (4H, t), 3.68 (12H, m), 3.85 (4H, t), 4.85 (2H, t). The ^{1}H NMR data of PEG-Si are as follows: δ0.68 (4H, t), 1.07 (18H, t), 1.85 (4H, m), 3.35 (4H, m), 3.42 (32H, t), 3.85 (12H, m), 4.25 (2H, t). From the ^{1}H NMR data of the precursor PEG-Si, it is proved that the polymerization degree of the polymer PEG is about 8–9, keeping consistent with the molecular weight of 380–430.

Synthesis of the hybrid materials (HMBA-G-Si-RE, HMBA-DG-Si-RE, HMBA-PEG-Si-RE): a stoichiometric amount of $Tb(NO_3)_3\cdot 6H_2O$ (1 mmol, 0.453 g) or $Eu(NO_3)_3\cdot 6H_2O$ (1 mmol, 0.446 g) was added into the precursor HMBA-Si dissolved in the absolute ethanol solution by stirring. After one hour, the precursor G-Si (DG-Si, PEG-Si) was added into the above mixture to coordinate to the rare earth ions. TEOS and H_2O were added into the mixture while stirring after 3 h, and then one drop of diluted hydrochloric acid was added to promote hydrolysis. The molar ratio of $RE(NO_3)_3\cdot 6H_2O$: HMBA-Si: G-Si (DG-Si, PEG-Si): TEOS: H_2O was 1:1:2:10:24. (TEOS 2.08 g; H_2O 0.432 g). After the treatment of hydrolysis, an appropriate amount of hexamethylenetetramine was added to adjust the pH to 6–7. The mixture was agitated magnetically to achieve a single phase in a covered Teflon beaker, and then it was aged at 70 °C until the onset of gelation in about 4 days. The hybrid materials containing organic aromatic ligand (HMBA-G-Si-RE, HMBA-DG-Si-RE and HMBA-PEG-Si-RE) were collected as monolithic bulks and ground into powdered material for the further studies (see Fig. 1b).

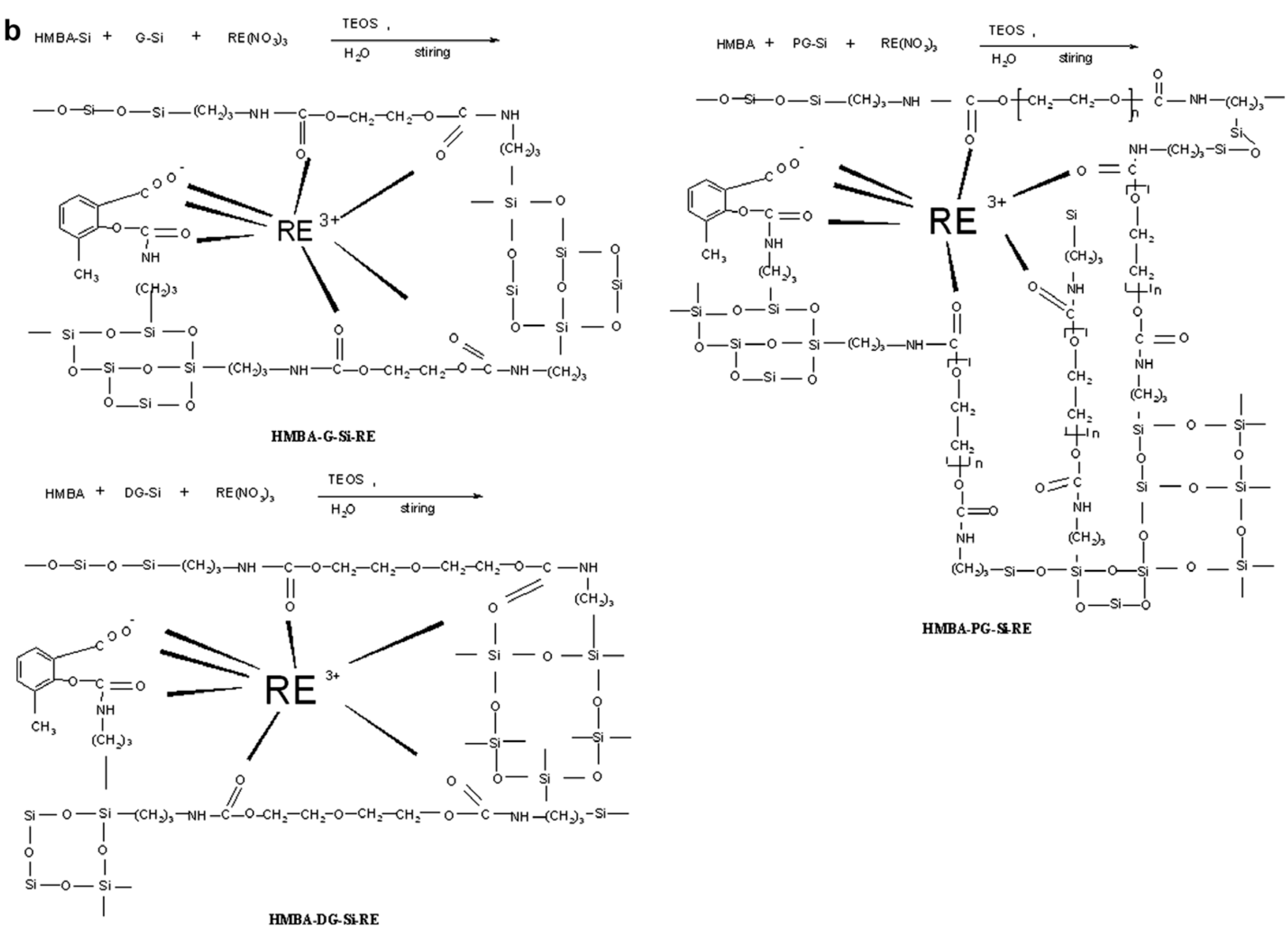

Fig. 1 (*continued*)

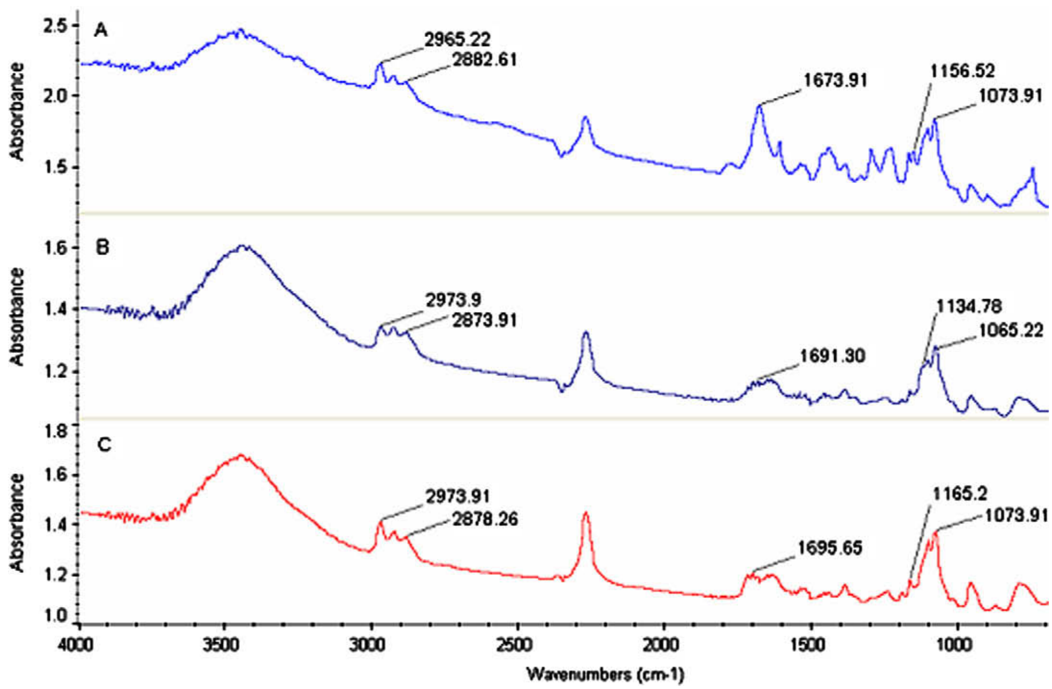

Fig. 2. The Fourier transform infrared spectra of the three precursors (A) HMBA-Si, (B) G-Si and (C) DG-Si.

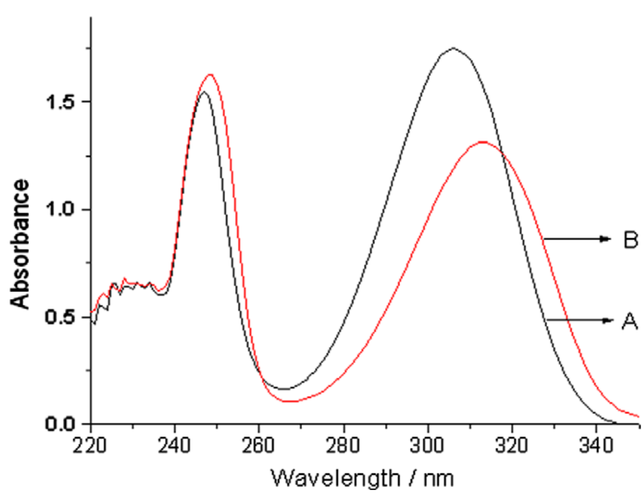

Fig. 3. The ultraviolet absorption spectra of the raw material (A) HMBA and the precursor (B) HMBA-Si.

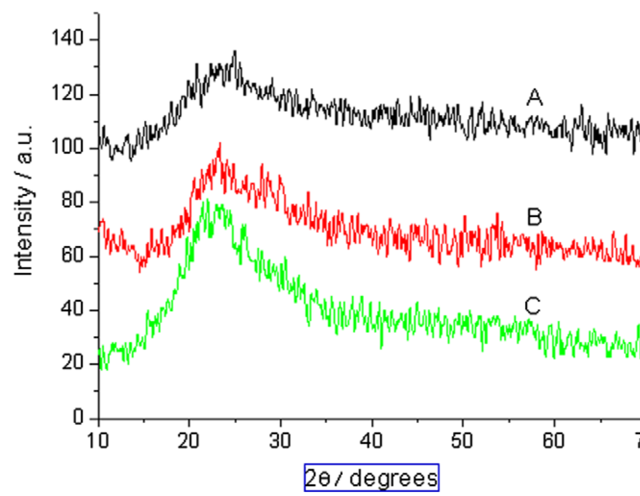

Fig. 4. The X-ray diffraction patterns for obtained hybrid materials A for HMBA-G-Si-Eu, B for HMBA-DG-Si-Eu and C for HMBA-PEG-Si-Eu.

2.3. Physical measurements

Infrared spectroscopy were obtained in KBr pellets and recorded on a Nexus 912 AO446 FT-IR spectrophotometer in the range of 4000–400 cm^{-1}. Ultraviolet absorption spectra (5×10^{-4} mol/L^{-1} using chloroform as solvent) and the ultraviolet–visible diffuse reflection spectra of the powder samples were recorded by an Agilent 8453 spectrophotometer and a BWS003 spectrophotometer, respectively. 1HNMR spectra were recorded in deuterate DMSO by a Bruker AVANCE-500 spectrometer with tetramethylsilane (TMS) as internal reference. The fluorescent excitation and emission spectra were obtained on a RF-5301 spectrophotometer: excitation slit width = 3 nm, emission slit width = 5 nm. Luminescence lifetime data were carried out on an Edinburgh FLS920 phosphorimeter using a 450 W xenon lamp as excitation source. The microstructure was estimated by scanning electronic microscope (SEM, Philips XL-30). The X-ray diffraction (XRD) measurements of the powdered sample were carried out by a BURKER D8 diffractometer (40 mA–40 kV) using monochromated Cu Kα1 radiation (k = 1.54 Å) over the 2θ range of 10–70°. All measurements were completed under the room temperature. Thermogravimetry (TG) was obtained on Netzsch, model STA 409C in the following conditions: nitrogen atmosphere, heating/cooling rate of 15 °C/min, 13.7 mg of powder; crucibles of Al_2O_3.

3. Results and discussion

3.1. Characterization of precursors

3.1.1. FI-IR spectra

The Fourier transform infrared spectra of (A) HMBA-Si, (B) G-Si and (C) DG-Si are shown in Fig. 2. The peaks at 1673 cm^{-1} (A),

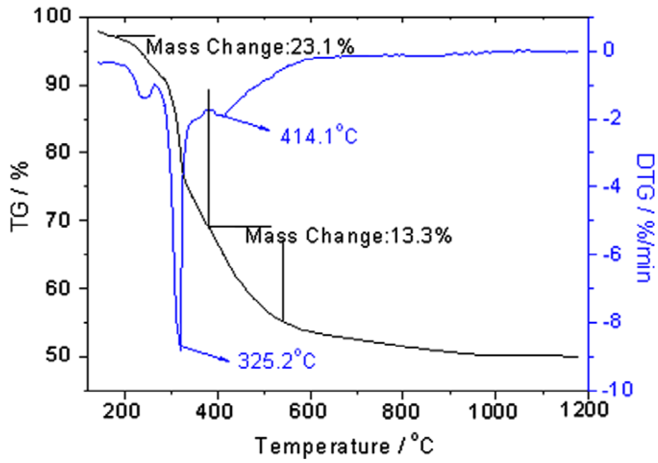

Fig. 5. The thermogravimetry trace (TG) of the obtained hybrid material HMBA-DG-Si-Tb.

$1693\ cm^{-1}$ (B) and $1695\ cm^{-1}$ (C) indicate the appearance of the amide groups (CONH), and the peaks located at $2965–2882\ cm^{-1}$ (A), $2973–2874\ cm^{-1}$ (B) and $2974–2878\ cm^{-1}$ (C) indicate the existence of the three methylene groups, both suggesting that 3-(triethoxysilyl)-propyl isocyanate (TEPIC) has been successfully grafted onto HMBA, glycol and diglycol, respectively, through the hydrogen transfer nucleophilic addition reaction between hydroxyl group of HMBA, glycol, diglycol and the isocyanate group of 3-(triethoxysilyl)-propyl isocyanate. The peaks located at $1156\ cm^{-1}$, $1134\ cm^{-1}$ and $1165\ cm^{-1}$ in A, B and C have attributed to the stretching vibration (Si–C), which also suggest the success of the graft reaction of 3-(triethoxysilyl)-propyl isocyanate (TEPIC) corresponding to the above conclusion, however the broad peak at $1039–1147\ cm^{-1}$ has emerged in A, B and C, relatively, indicating the stretching vibration of Si–O–Si possibly aroused by slight hydrolysis. Moreover, the wide band at about $3400\ cm^{-1}$ in the three spectra has been contributed by the overlap of the asymmetric and symmetric stretch (H–O–H) in the crystal water ($3600–3000\ cm^{-1}$), the double multiple absorption of C=O ($3500–3400\ cm^{-1}$) and N–H ($3500–3200\ cm^{-1}$).

3.1.2. Ultraviolet absorption spectra

Fig. 3 exhibits ultraviolet absorption spectra of the raw material (A) HMBA and the precursor (B) HMBA-Si. From the spectra, it is observed that the peaks at 247, 305 nm in A have shifted to 249, 314 nm in B with apparent red shift about 9 nm (A → B), which indicates the major $\pi–\pi^*$ electronic transition occurred in the precursor HMBA-Si, different from the former electronic transition in the ligand HMBA. It is estimated that the precursor HMBA-Si may promote the conjugated system in the more extensive rang and reduce the energy difference levels among electron orbits, so the electron distribution of the modified HMBA-Si has changed compared to free HMBA ligand due to the success of hydrogen transfer nucleophilic addition reaction between hydroxyl group of HMBA and the isocyanate group of TEPIC.

3.2. Characterization of hybrids

3.2.1. Powder XRD

The room-temperature X-ray diffraction patterns of the hybrid materials unfolded in Fig. 4 exhibit that the obtained hybrid materials are amorphous from 10° to 70°, (A) HMBA-G-Si-Eu, (B) HMBA-DG-Si-Eu and (C) HMBA-PEG-Si-Eu. The broad peaks all center on about 23.46° (structural unit distance 4.042 Å) in Eu^{3+}-containing hybrid materials due to the amorphous inorganic siliceous backbone of the Si–O network. In terms of the acceptance of the organic carbon chains bringing the regular order properties, the hybrid material should represent certain crystalline regions in these samples, but it was not shown in the figure due to the large amount of the host inorganic framework, whose amount is much more than the organic component. Moreover, it is illuminated that the addition of the organic aromatic ligand into hybrid material did not result in a decrease of the overall disorder of the siliceous skeleton and the polymeric carbon chains are subsequently in a disordered arrangement, but the polymeric carbon chains have brought some changes on electronic conjugate systems or coordination number of rare earth ions.

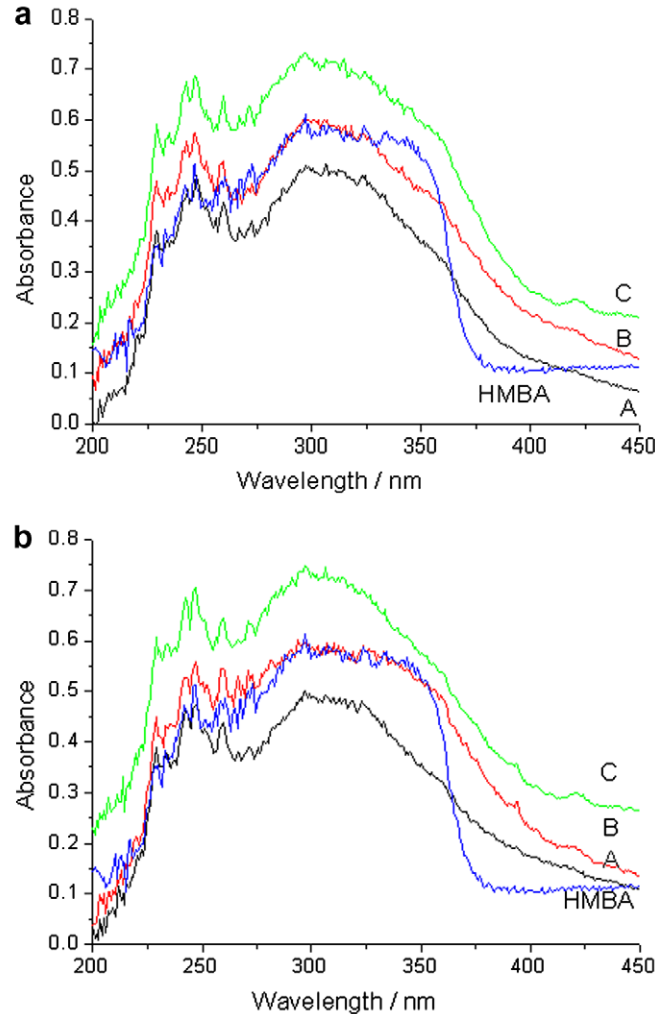

Fig. 6. The ultraviolet–visible diffuse reflection spectra of the raw material and hybrids. (A) HMBA-G-RE, (B) HMBA-DG-RE and (C) HMBA-PG-RE in (a) for terbium-containing and in (b) for europium-containing.

3.2.2. Thermal stabilities analysis

Fig. 5 shows the thermogravimetry trace (TG) and differential thermogravimetry trace (DTG) of the hybrid material HMBA-DG-Si-Tb. Seen from the TG curve of the hybrid material HMBA-DG-Si-Tb there exists a mass loss (23.96%) with the heat flow around 325.2 °C which has been shown in the DTG curve. It is speculated that the mass loss has mostly attributed to the decomposition of the organic aromatic ligand HMBA, which occupies 19.55% of the molecular weight HMBA-DG-Si-Tb according to the molecular structure. In addition, a minor mass loss (4.41%) has been assigned to the escape process of the solvent DMF and a small part of organic component from DG-Si. Furthermore, the hybrid lost the weight of 13.3% at 414.1 °C basically attributing to the intense rupture and decomposition of several organic segments of DG-Si. At last the hybrid retains the mass (about 57.60%) until 1300 °C, which is almost half of the whole weight. Since the weight of the precursor DG-Si possesses 58.67% in the hybrid, the final data have indicated that the residue is composed of the plentiful inorganic Si–O network and a small quantity of the precursor of DG-Si. It is concluded the hybrid material HMBA-DG-Si-Tb provides its own outstanding thermal stabilities, since the organic aromatic ligand HMBA coordinates to the center metal ion with the precursor DG-Si simultaneously to assemble the luminescent hybrid materials possessing the silicon–oxygen networks and the organic carbon–oxygen chains together, which has brought more efficient conjugated system and thermal stabilities.

3.2.3. Ultraviolet–visible diffuse reflection spectra

The ultraviolet–visible diffuse reflection spectra of the hybrid materials are given in Fig. 6a for Tb^{3+} and (b) for Eu^{3+}. The lines A, B, C and HMBA denote the rare earth hybrid materials and the free ligand (A for HMBA-G-Si-RE, B for HMBA-DG-Si-RE, C for HMBA-PEG-Si-RE and HMBA for 2-hydroxyl-3-methylbenzoic acid). It is observed that the wide band of HMBA is located at about 280–340 nm and the wide bands of the hybrid materials are located at about 270–350 nm in (a) and 275–360 nm in (b), which partially overlap with the fluorescence excitation spectra (wide bands at 280–360 nm in Fig. 8a and at 350–450 nm in Fig. 8b). It can be predicted that the ligand or precursors have absorbed abundant energy in ultra-visible extent to transfer the energy to the rare earth ions and the intramolecular energy transfer has been completed efficiently. Then the final hybrid materials can be expected to have relative excellent luminescence properties, which are proved in the fluorescence spectra in Fig. 8. Ulteriorly, the spectra of these two groups of the hybrid materials with the different center metal ions show a little difference on the peak shape, which has been presumed that different internal configurations of the hybrid materials has some influence on the energy absorption in ultra-visible extent and on intramolecular energy transfer coefficient.

3.2.4. Microstructure analysis by scanning electron micrographs

The scanning electron micrographs for the six kinds of hybrid materials demonstrate that the homogeneous, molecular-based materials were obtained with covalent bonds between the organic ligand or the polymer and the inorganic matrix, which belongs to a complicated huge molecular system (see Fig. 7) (a) for HMBA-G-Si-Tb, (b) for HMBA-DG-Si-Tb, (c) for HMBA-PEG-Si-Tb (d) for HMBA-G-Si-Eu, (e) for HMBA-DG-Si-Eu and (f) for HMBA-PEG-Si-Eu.

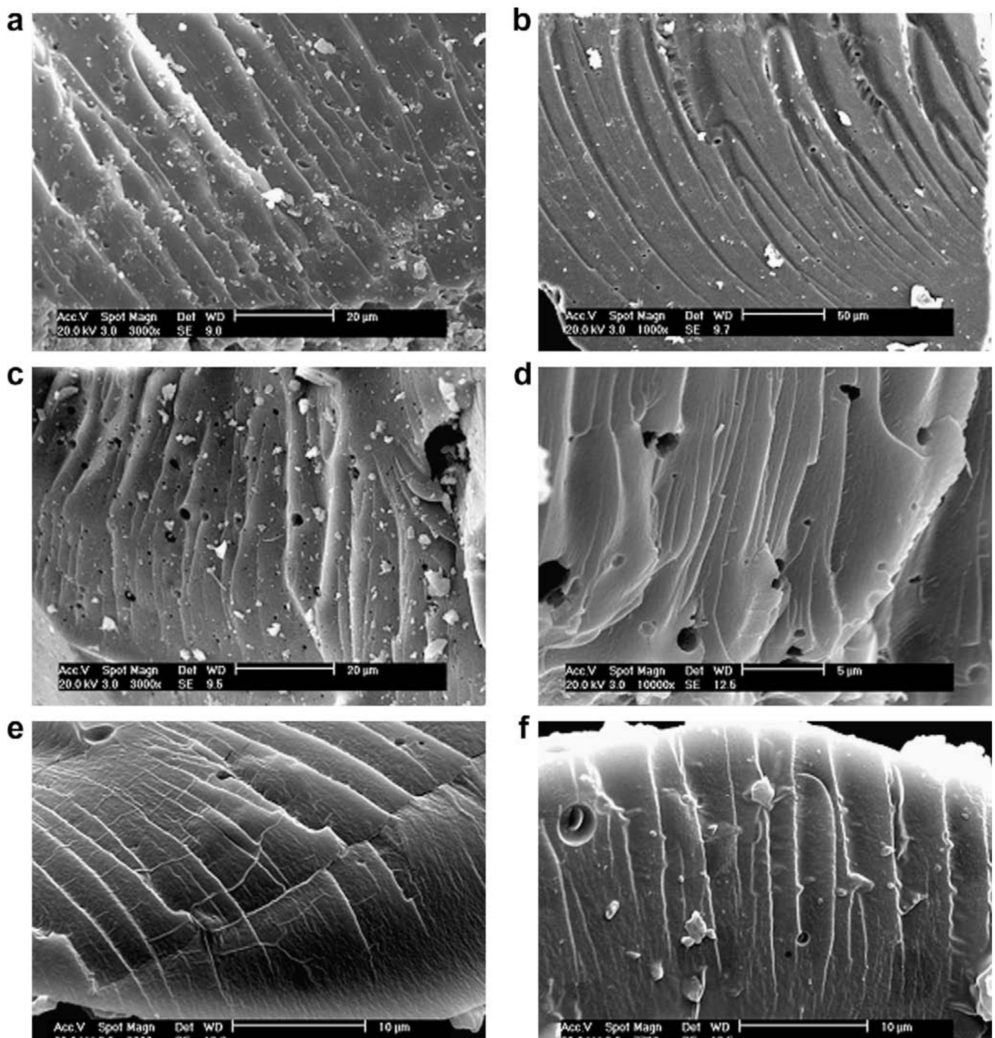

Fig. 7. SEM images of the hybrid materials (a) for HMBA-G-Si-Tb, (b) for HMBA-DG-Si-Tb, (c) for HMBA-PEG-Si-Tb (d) for HMBA-G-Si-Eu, (e) for HMBA-DG-Si-Eu and (f) for HMBA-PEG-Si-Eu.

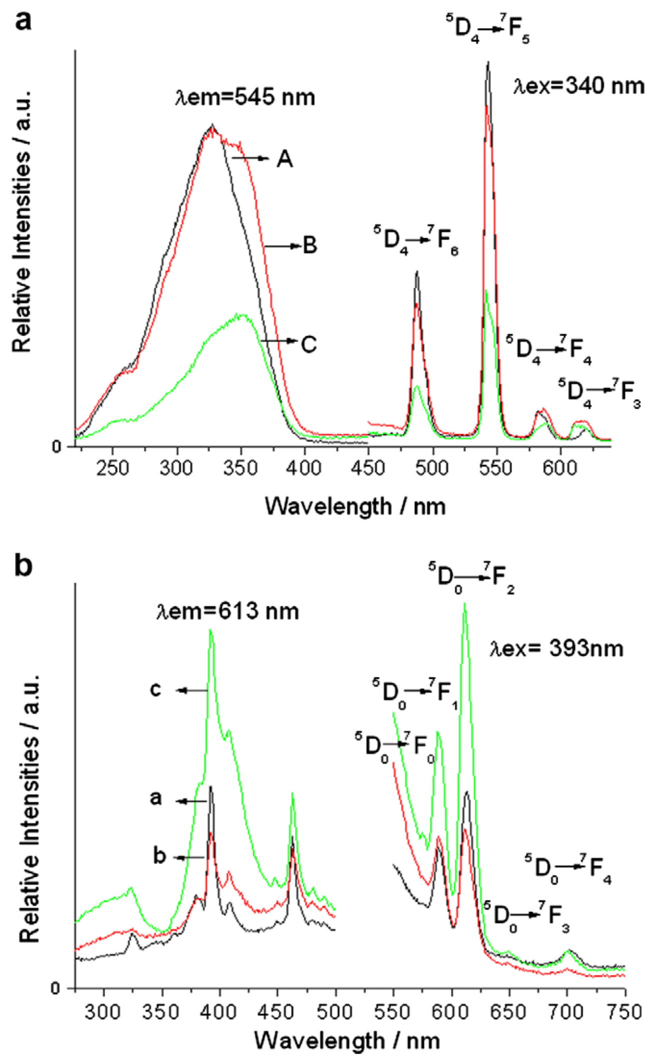

Fig. 8. The excitation and emission spectra of the hybrid materials (A) HMBA-G-Si-Tb, (B) HMBA-DG-Si-Tb and (C) HMBA-PEG-Si-Tb in a; (a) HMBA-G-Si-Eu, (b) HMBA-DG-Si-Eu and (c) HMBA-PEG-Si-Eu in b.

Compared with the hybrid material with doped lanthanide complexes which generally experiences the phase separation phenomena, in this paper the inorganic and organic phases can combine their distinct properties together in the hybrid materials we obtained without the phase separation.

The precursor HMBA-Si is a derivative from 2-hydroxy-3-methylbenzoic acid (aromatic carboxylic acids), and its corresponding complex may be ready to form one-dimensional chain-like polymeric structure and retain the coordination position in the hybrid materials synthesized later. Therefore, when the precursor HMBA-Si coordinates to the Tb^{3+} or Eu^{3+}, it is easy to form the one-dimensional chain-like microstructure, which competes with the construction of the polymeric network structure of Si–O–Si in hydrolysis/polycondensation process. Subsequently, it is seen from the micrographs that the tendency to form the polymeric network of Si–O–Si plays a primary role to result in the final structure and morphology: on the surface of each kind of these hybrid materials there exist homogeneous bulk trunks or stripes of pine-like microstructure with regular orders. The tiny phenomena attracting us is that there are some embranchments at the end of each stripe and the stripes will continue to extend according to the former directions of these embranchments, which forms the final structure as we have seen in the micrographs. Therefore, it is also summarized that the tendency to form the polymeric Si–O–Si network has become the primary tendency when it competed with the tendency to form one-dimensional chain-like structure. In addition, besides the bulk trunk or stripe of pine-like microstructure, it has shown that many large pore-like holes with the same size about 1 μm are dispersed on the backbone of the bulk trunk of the six kinds of materials. It is speculated that the pin-holes microstructure might be formed by the hugely different thermal expansion coefficient between the aromatic ligand and silica during the hydrolysis/polycondensation process between HMBA-Si, the G-Si, DG-Si, PEG-Si and TEOS or the evaporation of solvent in the thermal and aging procedure. Ulteriorly, seen form the Fig. 7f, it is shown that on the surface there exist plenty of regular circles which have not penetrated through the surfaces. The reason is speculated that there is no enough time for the planar circles to form the pin-holes in the synthesis and hydrolysis/polycondensation processes. Therefore, the moiety of the organic aromatic ligand has played an important role in the preparation of the Tb^{3+}, Eu^{3+}-containing hybrid material and the combination of the organic ligand, long carbon chains and the inorganic silicon–oxygen network could induce the pin-hole-like microstructure formed on the surface.

3.2.5. Photoluminescence spectra

According to the energy transfer and intramolecular energy mechanism [40–42], the most important factor for the luminescence property of rare earth complex is the intramolecular energy transfer efficiency, which mainly depends on two energy transfer processes [43]. One is from lowest triplet level of ligand to the emissive level of Ln^{3+} (rare earth ion) mentioned in Dexter's resonant exchange interaction theory [44,45]; the other is the reverse energy transition derived from the thermal deactivation mechanism. And the energy transfer rate constant (K_T) is dependent on the energy difference ($\Delta E_{(}$Tr—Ln^{3+})) between the lowest triplet level energy of ligand and the resonant emissive level energy of the central Ln^{3+}. Based on the above mechanism, the conclusion can be drawn that the energy level difference $\Delta E_{(}$Tr—Ln^{3+}) have vital influence on the energy transfer process, and there should be an optimal energy difference between the triplet level of ligand and the emissive level of terbium and europium ions in the hybrid polymeric materials. If the energy difference is too large, the energy-transfer rate constant will decrease due to the diminution on the overlap between the energy level of the donor (HMBA) and the acceptor (Tb^{3+} or Eu^{3+}). On the contrary, if the energy difference is too small, the energy could be back-transferred to the triplet state of the ligand [46]. The resonance level energy of Eu^{3+} ($^5D_1$) is 19020 cm^{-1} and that of Tb^{3+} ($^5D_4$) is 20 430 cm^{-1} [40], and the lowest triplet state level energy of the ligand HMBA is 22 730 cm^{-1} obtained from the phosphorescence data, which is higher than both of resonance level energy of Eu^{3+} and Tb^{3+}. And through the calculation, the energy difference is 2300 cm^{-1} between the lowest triplet state level energy of HMBA and Tb^{3+}, while 3710 cm^{-1} for Eu^{3+}, so the triplet state energy of HMBA is predicted to be more suitable for Tb^{3+} than Eu^{3+}. Furthermore, the efficient intramolecular energy transfer mechanism in the hybrid polymeric materials containing Tb^{3+} will operate more efficiently than that in materials containing Eu^{3+}, which has been proved by the luminescent spectra as follow.

The fluorescent excitation and emission spectra of the hybrid materials are shown in Fig. 8a and b. The excitation spectra were obtained by monitoring the emission of Tb or Eu ion at 543 or 613 nm. The spectra were dominated by a broad band centered at about 350 nm for Tb ion, which is assigned to the absorption of ligand indicating that the intramolecular energy transfer has completed efficiently, while a narrow peak centered at 393 nm for Eu ion ascribes to the characteristic absorption of the f–f transitions, which shows the intramolecular energy transfer has not completed efficiently due to the unsuitable energy match between the ligand and the Eu ion motioned in the above discussion. The emission lines of the hybrid materials are assigned to the transitions from the $^5D_4 \rightarrow {^7F_J}$ ($J = 6, 5, 4, 3$) transitions at about 486, 543, 583 and 619 nm for Tb ion in (a) and $^5D_0 \rightarrow {^7F_J}$ ($J = 0, 1, 2, 3, 4$) transitions at about 575, 589, 612, 648 and 701 nm for Eu ion in (b), respectively. In Fig. 8a the green emission intensities are the strongest of all the emission of Tb^{3+}-containing hybrid material, which can be explained by the conclusion that the leaching of the photoactive molecules is avoided and a higher concentration of emitting metal ions is obtained. Therefore, it is indicated that the effective energy transfer took place between the four precursors (HMAB-Si, G-Si, DG-Si and PEG-Si) and the chelated rare earth ions. And seen from Fig. 8b, among these emission peaks of the Eu^{3+}-containing hybrid material, red emission intensities (arbitrary unit, a.u.) of electric dipole transition of $^5D_0 \rightarrow {^7F_2}$ at about 613 nm (208.2 for a, 168.9 for b and 406.9 for c) are larger than the orange emission intensities of magnetic dipole transition of $^5D_0 \rightarrow {^7F_1}$ at about 589 nm (148.8 for a, 160.3 for b and 272.0 for c), respectively, which indicates Eu ion is located in an environment without inversion symmetry [47,48]. Although the effective energy transfer has not operated between the four precursors and the chelated Eu^{3+} as well as that between the four precursors and chelated Tb^{3+}, the hybrid materials indeed show some certain fluorescent emission spectra. Some factors for the luminescence may not be excluded such as relatively rigid structure of silica gel which limits the vibration of ligand in the hybrid materials and prohibits non-radiative transitions.

Furthermore, it is seen from the spectra (a) and (b) that the line A shows a little large relative fluorescent intensities than B or C in (a), while in (b) the line c gives the largest relative fluorescent intensities. Following Dexter's exchange energy transfer theory [44]: the luminescence intensities of hybrid materials depend on the matching degree of the ligand's triplet state energy and lanthanide ion's emission energy, the reason has been speculated that the energy matching degree between the resonant emissive energy level of Tb^{3+} and the triplet state energy of the precursors G-Si and HMBA-Si is better than the others in (a), while in (b) the energy matching between the resonant emissive energy level of Eu^{3+} and the triplet state energy of the precursors PEG-Si and HMBA-Si is the most successful. And another potential reason is that the hybrid material HMBA-PEG-Si-Eu possesses the long carbon chains while the others do not, which induces that the final material has been assembled to be a molecular hybrid polymeric material with the silicon–oxygen networks and the carbon chains at the same time so as to sensitize the rare earth ions more effectively.

3.2.6. Luminescence decay times (τ) and emission quantum efficiency (η)

The typical decay curve of the Eu and Tb hybrid materials were measured and they can be described as a single exponential ($\mathrm{RE}(S(t)/S_0) = -k_1 t = -t/\tau$), indicating that all Eu^{3+} and Tb^{3+} ions occupy the same average coordination environment. For terbium hybrids, the luminescent lifetime of HMBA-G-Si-Tb (0.45 ms) is longer than that of HMBA-DG-Si-Tb (0.18 ms) and HMBA-PEG-Si-Tb (0.10 ms) (see Supporting information Table S1 and Fig. S1). But the luminescent efficiency of terbium hybrids can not be determined exactly and directly from the luminescence lifetimes and spectra because Tb^{3+} has not the completely isolated magnetic dipolar transition like $^5D_0 \rightarrow {^7F_1}$ transition of Eu^{3+}.

According to the emission spectra and the lifetime of the Eu^{3+} first excited state level (τ, $^5D_0$), the emission quantum efficiency (η) of the $^5D_0$ excited state can be determined. Assuming that only non-radiative and radiative processes are essentially involved in the depopulation of the $^5D_0$ state, η can be defined as follows [49]:

$$\eta = \frac{A_r}{A_r + A_{nr}} \tag{1}$$

Here, A_r and A_{nr} are radiative and non-radiative transition rates, respectively. A_r can be obtained by summing over the radiative rates A_{0J} for each $^5D_0 \rightarrow {^7F_J}$ ($J = 0$–4) transitions of Eu^{3+}

$$A_r = \sum A_{0J} = A_{00} + A_{01} + A_{02} + A_{03} + A_{04} \tag{2}$$

The branching ratio for the $^5D_0 \rightarrow {^7F_{5,6}}$ transitions can be neglected as they are not detected experimentally, whose influence can be ignored in the depopulation of the $^5D_0$ excited state. Since $^5D_0 \rightarrow {^7F_1}$ belongs to the isolated magnetic dipole transition, it is independent of the chemical environment around the Eu^{3+}, and thus can be considered as an internal reference for the whole spectra, the experimental coefficients of spontaneous emission, A_{0J} can be calculated according to the equation [50–52]

$$A_{0J} = A_{01}(I_{0J}/I_{01})(\upsilon_{0J}/\upsilon_{0J}) \tag{3}$$

Here, A_{0J} is the experimental coefficients of spontaneous emission. A_{01} is the Einstein's coefficient of spontaneous emission between the $^5D_0$ and $^7F_1$ energy levels. In vacuum, A_{01} as a value of $14.65\ s^{-1}$, when an average index of refraction n equal to 1.506 was considered, the value of A_{01} can be determined to be $50\ s^{-1}$ approximately ($A_{01} = n^3 A_{01(\mathrm{vac})}$) [53]. I_{01} and I_{0J} are the intensities of the $^5D_0 \rightarrow {^7F_1}$ and $^5D_0 \rightarrow {^7F_J}$ transitions ($J = 0$–4) with v_{01} and v_{0J} ($v_{0J} = 1/\lambda_J$) energy centers, respectively. υ_{0J} refers to the energy barycenter and can be determined from the Eu^{3+}'s $^5D_0 \rightarrow {^7F_J}$ emission transitions. The emission intensity, I, taken as integrated intensity S of the $^5D_0 \rightarrow {^7F_{0-4}}$ emission curves, can be defined as below:

$$I_{i-j} = \hbar\omega_{i-j} A_{i-j} N_i \approx S_{i-j} \tag{4}$$

Here, i and j are the initial ($^5D_0$) and final levels ($^7F_{0-4}$), respectively, ω_{i-j} is the transition energy, A_{i-j} is the Einstein's coefficient of spontaneous emission, and N_i is the population of the $^5D_0$ emitting level. On the basis of Refs. [54–57], the value of A_{01} ($\approx 50\ s^{-1}$) and the lifetime (τ), radiative (A_r), and non-radiative (A_{nr}) transition rates are correlative in the following equation:

$$A_{tot} = 1/\tau = A_r + A_{nr} \tag{5}$$

On the basis of the above discussion, the quantum efficiencies of the three kinds of europium hybrid materials can be determined, as shown in Table 1. In the equation of η, it can be seen the value η mainly depends on the values of two factors: one is lifetimes and the other is I_{02}/I_{01}. Since the intensities of the transitions $^5D_0 \rightarrow {^7F_1}$ and $^5D_0 \rightarrow {^7F_2}$ are larger than those of other transitions, the ration of I_{02}/I_{01} has the most important influence on the A_J. The quantum efficiencies of the hybrid material (HMBA-G-Si-Eu) are higher than the other materials seen from Table 1, since it has the shortest carbon chains so that there was less steric exclusion effect in the coordination procedure, resulting in that the molecular configuration has been formed more easily and stable than the others.

However, although the hybrid material (HMBA-PEG-Si-Eu) has the largest radiative rate (A_r), while its lifetime is the smallest of the three hybrids, it has not shown the relative high quantum efficiencies. We have speculated that the longer carbon chains with steric exclusion effect have played a crucial role on the luminescence decay process.

Furthermore, we determined the Judd–Ofelt Parameters for the three covalently bonded europium hybrid materials. The spontaneous emission probability A of the transition is related to its dipole strength according to Eq. (6) [54–57]

$$A = (64\pi^4\upsilon^3)/[3h(2J+1)][(n^2+2)^2/9n]S_{(\mathrm{ED})} + n^2 S_{(\mathrm{MD})} \tag{6}$$

υ is the average transition energy in cm^{-1}, h is Planck constant, $2J + 1$ is the degeneracy of the initial state (1 for $^5D_0$). $S_{(\mathrm{ED})}$ and

Table 1
The luminescence efficiencies and lifetimes of the solid covalent hybrids.

Hybrid systems	HMBA-G-Si-Eu	HMBA-DG-Si-Eu	HMBA-PEG-Si-Eu
υ_{00} (cm^{-1})[a]	17 381	17 345	17 381
υ_{01} (cm^{-1})[a]	16 966	16 976	17 002
υ_{02} (cm^{-1})[a]	16 299	16 345	16 340
υ_{03} (cm^{-1})[a]	15 429	15 431	15 403
υ_{04} (cm^{-1})[a]	14238	14 233	14 274
I_{00}[b]	64	103	141
I_{01}[b]	148	160	272
I_{02}[b]	208	168	406
I_{03}[b]	12	17	19
I_{04}[b]	17	10	19
I_{02}/I_{01}[b]	1.41	1.05	1.49
A_{00} (s^{-1})	21.11	31.50	25.35
A_{01} (s^{-1})	50.00	50.00	50.00
A_{02} (s^{-1})	73.15	54.53	77.66
A_{03} (s^{-1})	4.46	5.84	3.86
A_{04} (s^{-1})	6.84	3.73	4.16
τ (ms)[c]	0.36	0.30	0.29
A_{rad} (s^{-1})	155.55	145.60	161.03
τ_{exp}^{-1} (s^{-1})	2741.23	3282.99	3448.28
A_{nrad} (s^{-1})	2585.68	3137.39	3287.25
η (%)	5.68	4.44	4.67
Ω_2 ($\times 10^{-20}$ cm^2)	2.12	1.58	2.25
Ω_4 ($\times 10^{-20}$ cm^2)	0.46	0.25	0.28

[a] The energy barycenters of the $^5D_0 \rightarrow {}^7F_J$ transitions (υ_{0J}).
[b] The integrated intensities of the $^5D_0 \rightarrow {}^7F_J$ emission curves.
[c] For $^5D_0 \rightarrow {}^7F_2$ transition of Eu^{3+}.

$S_{(MD)}$ are the electric and magnetic dipole strengths, respectively. The factors containing the medium's refractive index n result from local field corrections that convert the external electromagnetic field into an effective field at the location of the active center in the dielectric medium. Moreover, the transitions from $^5D_0$ to $^7F_{0,3,5}$ ($J = 0, 3, 5$) are forbidden both in magnetic and induced electric dipole schemes ($S_{(MD)}$ and $S_{(ED)}$ are zero). The transition from $^5D_0$ to $^7F_1$ ($J = 1$) is the isolated magnetic dipole transition and has no electric dipole contribution, which practically independent of the ion's chemical environment and can be used as a reference as above mentioned. Besides, the $^5D_0 \rightarrow {}^7F_6$ transition could not be experimentally detected and it is not necessary to determine its J–O parameter. So we only need to estimate the two parameters (Ω_2, Ω_4) related to the two purely induced electric dipole transitions $^5D_0 \rightarrow {}^7F_{2,4}$ on basis of only three parameters Ω_λ using Eq. (7) [54–57]

$$A = (64e^2\pi^4\upsilon^3/[3h(2J+1)][(n^2+2)^2/9n]\sum \Omega_\lambda|\langle^5D_0)||U^{(\lambda)}||^7F_J\rangle^2 \quad (7)$$

where e is the electronic charge. With the refraction index $n = 1.506$, and $\langle^5D_0||U^{(\lambda)}||^7F_J\rangle^2$ values are the square reduced matrix elements whose values are 0.0032 and 0.0023 for $J = 2$ and 4, respectively. The Ω_2, Ω_4 intensity parameters for the three hybrid materials are shown in Table 1. The distinction between the two intensity parameters for each hybrid is not apparent, suggesting that the Eu^{3+} is located in a polarizable chemical environment for luminescence.

4. Conclusion

We have developed a representative method for assembling the luminescent rare earth molecular-based polymeric hybrid materials with chemical bonds, which contain long organic polymeric carbon chains and organic network (Si–O–Si) through sol–gel process. The precursor HMBA-Si, G-Si, DG-Si and PEG-Si were constructed through the hydrogen transfer nucleophilic addition reaction between hydroxyl groups and the isocyanate groups. Then the final hybrids were synthesized after the coordination and hydrolysis and polycondensation processes. Furthermore, the photoluminescence properties, SEM diagraphs and thermogravimetry results illuminate that the different conjugated configurations and coordination numbers may result in the different intramolecular energy transfer systems and have the important influence on the luminescent properties. Furthermore, all kinds of hybrids obtained possess thermodynamic stabilities and uniform microstructures due to their self-assembly mechanism. Therefore, these kinds of homogeneous molecular-based polymeric hybrid materials can be expected to have potential and significant application in optical and electronic devices in the future.

Acknowledgements

This work was supported by the National Natural Science Foundation of China (20671072) and Program for New Century Excellent Talents in University (NCET-08-0398).

Appendix A. Supplementary data

Supplementary data associated with this article can be found, in the online version, at doi:10.1016/j.jorganchem.2009.06.019.

References

[1] M. Elbanowshi, B. Makowska, J. Photochem. Photobiol. 99 (1996) 85–92.
[2] E. Soini, Trends Anal. Chem. 9 (1990) 90–93.
[3] J. Kido, H. Hayase, K. Hongawa, K. Nagai, K. Okuyama, Appl. Phys. Lett. 65 (1994) 2124–2126.
[4] N. Sabbatini, M. Guardigli, J.M. Lehn, Coord. Chem. Rev. 123 (1993) 201–228.
[5] Q.J. Zhang, P. Wang, X.F. Sun, Y. Zhai, P. Dai, Appl. Phys. Lett. 72 (1998) 407–409.
[6] R.J. Mears, L. Reekie, I.M. Jauncey, D.N. Payne, Electron. Lett. 22 (1986) 159–160.
[7] T. Suratwala, Z. Gardlund, K. Davidson, D.R. Uhlmann, Chem. Mater. 10 (1998) 190–198.
[8] C. Molina, K. Dahmouche, C.V. Santilli, Chem. Mater. 13 (2001) 2818–2823.
[9] B. Alpha, R. Ballardini, V. Balzani, J.M. Lehn, S. Perathoner, N. Sabbatini, Angew. Chem., Int. Ed. Engl. 26 (1987) 299–302.
[10] C. Sanchez, F. Ribot, New J. Chem. 18 (1994) 1007–1047.
[11] J.H. Harreld, A. Esaki, G.D. Stucky, Chem. Mater. 15 (2003) 3481–3489.
[12] P.N. Minoofar, R. Hernandez, S. Chia, B. Dunn, J.I. Zink, A.C. Franville, J. Am. Chem. Soc. 124 (2002) 14388–14396.
[13] A.C. Franville, D. Zambon, R. Mahiou, Y. Troin, Chem. Mater. 12 (2000) 428–435.
[14] B. Yan, H.F. Lu, Inorg. Chem. 47 (2008) 5601–5611.
[15] A.C. Franville, R. Mahiou, D. Zambon, J.C. Cousseins, Solid State Sci. 3 (2001) 211–222.
[16] H.R. Li, J. Lin, H.J. Zhang, L.S. Fu, Q.G. Meng, S.B. Wang, Chem. Mater. 14 (2002) 3651–3655.
[17] H.R. Li, J. Lin, H.J. Zhang, H.C. Li, L.S. Fu, Q.G. Meng, Chem. Commun. (2001) 1212–1213.
[18] Q.M. Wang, B. Yan, J. Mater. Chem. 14 (2004) 2450–2455.
[19] D.W. Dong, S.C. Jiang, Y.F. Men, X.L. Ji, B.Z. Jiang, Adv. Mater. 12 (2000) 646–649.
[20] J.C. Boyer, F. Vetrone, J.A. Capobianco, A. Speghini, M. Bettinelli, J. Phys. Chem. B 108 (2004) 20137–20144.
[21] Y. Li, B. Yan, J. Solid State Chem. 181 (2008) 1032–1039.
[22] B. Yan, D.J. Ma, J. Solid State Chem. 179 (2006) 2059–2066.
[23] Y. Li, B. Yan, H. Yang, J. Phys. Chem. C 112 (2008) 3959–3968.
[24] J.L. Liu, B. Yan, J. Phys. Chem. C 112 (2008) 14168–14178.
[25] F.Y. Liu, L.S. Fu, H.J. Zhang, New J. Chem. 27 (2003) 233–236.
[26] L.D. Carlos, R.A. Sá Ferreira, R.N. Pereira, M. Assuncao, V.D. Bermudez, Phys. Chem. B 108 (2004) 14924–14932.
[27] L.D. Carlos, Mol. Phys. 101 (2003) 1037–1045.
[28] M. Kawa, J.M.J. Frechet, Chem. Mater. 10 (1998) 286–296.
[29] L.R. Matthews, E.T. Knobbe, Chem. Mater. 5 (1993) 1697–1700.
[30] Q.M. Wang, B. Yan, J. Photochem. Photobiol. A: Chem. 177 (2006) 1–5.
[31] B. Yan, L.M. Zhao, J.L. Liu, J. Photochem. Photobiol. A. Chem. 199 (2008) 50–56.
[32] B. Yan, Q.M. Wang, J. Photochem. Photobiol. A Chem. 197 (2008) 213–219.
[33] V. Bekiari, G. Pistolis, P. Lianos, Chem. Mater. 11 (1999) 3189–3196.
[34] L.H. Wang, W. Wang, W.G. Zhang, E.T. Kang, W. Huang, Chem. Mater. 12 (2002) 2212–2219.
[35] J.R. MacCallum, C.A. Vincent (Eds.), Polymer Electrolyte Reviewss1, Elsevier Applied Science, London, 1987.
[36] R.G. Linford (Ed.), Electrochemical Science and Technology of Polymers 1, Elsevier Applied Science, London, 1987.

[37] F.M. Gray, Solid Polymer Electrolytes: Fundamentals and Technological Applications, VCH, New York, 1991.
[38] R.G. Linford (Ed.), Electrochemical Science and Technology of Polymers 2, Elsevier Applied Science, London, 1991.
[39] M.B. Armand, Adv. Mater. 2 (1990) 278–282.
[40] S. Sato, W. Mada, Bull. Chem. Soc. 43 (1970) 1955–1966.
[41] G.A. Crosby, R.E. Whan, R.M. Alire, J. Chem. Phys. 34 (1961) 743–745.
[42] B. Yan, H.J. Zhang, S.B. Wang, J.Z. Ni, J. Photochem. Photobiol. A Chem. 112 (1998) 209–214.
[43] B. Yan, B. Zhou, J. Photochem. Photobiol. A: Chem. 171 (2005) 181–186.
[44] D.L. Dexter, J. Chem. Phys. 21 (1953) 836–839.
[45] Q.M. Wang, B. Yan, X.H. Zhang, J. Photochem. Photobiol. A: Chem. 174 (2005) 119–124.
[46] B. Yan, Y.S. Song, J. Fluorescence 14 (2004) 289–294.
[47] C.R.S. Dean, T.M. Shepherd, J. Chem. Soc., Faraday Trans. II 71 (1975) 146–150.
[48] Y. Hasegawa, M. Yamamuro, Y. Wada, N. Kanehisa, Y. Kai, S. Yanagida, J. Phys. Chem. A 107 (2003) 1697–1702.
[49] R.A. Sa' Ferreira, L.D. Carlos, R.R. Gonçalves, S.J.L. Ribeiro, V.D. Bermudez, Chem. Mater. 13 (2001) 2991–2998.
[50] B. Yan, X.F. Qiao, J. Phys. Chem. B 111 (2007) 12362–12374.
[51] P.C.R. Soares-Santos, H.I.S. Nogueira, V. Felix, M.G.B. Drew, Chem. Mater. 15 (2003) 100–108.
[52] E.E.S. Teotonio, J.G.P. Espynola, H.F. Brito, O.L. Malta, S.F. Oliveria, D.L.A. de Foria, C.M.S. Izumi, Polyhedron 21 (2002) 1837–1844.
[53] L.D. Carlos, Y. Messaddeq, H.F. Brito, Adv. Mater. 12 (2000) 594–598.
[54] M.F. Hazenkamp, G. Blasse, Chem. Mater. 2 (1990) 105–110.
[55] M.H.V. Werts, R.T.F. Jukes, J.W. Verhoeven, Phys. Chem. Chem. Phys. 4 (2002) 1542–1548.
[56] O.L. Malta, H.F. Brito, J.F.S. Menezes, J. Lumin. 75 (1997) 255–268.
[57] G.F. de Sa, O.L. Malta, Coord. Chem. Rev. 196 (2000) 165–195.